ECCOMAS Congress 2016
VII European Congress on Computational Methods in Applied Sciences and Engineering
M. Papadrakakis, V. Papadopoulos, G. Stefanou, V. Plevris (eds.)
Crete Island, Greece, 5–10 June 2016

PASSIVE CONTROL OF WAVE PROPAGATION IN PERIODIC ANTI-TETRACHIRAL META-MATERIALS

Marco Lepidi[1], **Andrea Bacigalupo**[2]

[1]DICCA Department of Civil, Chemical and Environmental Engineering, University of Genova
Via Montallegro, 1 - 16145 Genova (Italy)
e-mail: marco.lepidi@unige.it

[2] IMT School for Advanced Studies Lucca
Piazza S. Francesco, 19 - 55100 Lucca (Italy)
e-mail: andrea.bacigalupo@imtlucca.it

Keywords: Auxetic materials, Wave propagation, Resonators, Meta-materials, Passive control

Abstract. *Periodic anti-tetrachiral materials are strongly characterized by a marked auxeticity, the unusual and fascinating mechanical property mathematically expressed by negative values of the Poisson's ratio. The auxetic behavior is primarily provided by pervasive rolling-up mechanisms developed by the doubly-symmetric micro-structure of the periodic cell, composed by a regular pattern of rigid rings connected by tangent flexible ligaments. Adopting a beam-lattice model to describe the linear free dynamics of the elementary cell, the planar wave propagation along the bi-dimensional material domain can be studied according to the Floquet-Bloch theory. Parametric analyses of the dispersion curves, carried out with numerical or asymptotic tools, typically reveal a highly-dense spectrum, with persistent absence of total band-gaps in the low-frequency range. The paper analyses the wave propagation in the meta-material developed by introducing rigid massive inserts, locally housed by all the rings and working as undamped linear oscillators with assigned inertia and/or stiffness properties. The elastic coupling between the cell microstructure and the oscillators, if properly tuned (inertial resonators), is found to significantly modify the Floquet-Bloch spectrum of the material. The effects of the resonator parameters (tuning frequency and mass ratio) on the low-frequency band structure of the meta-material are discussed, with focus on the valuable possibility to (i) open total band gaps, by either the widening of an existing partial band gap or the avoidance of a crossing point between adjacent dispersion curves, (ii) finely control the total band-gap amplification, in order to assess the maximum achievable performance of the meta-material against the vibration propagation.*

1 INTRODUCTION

Auxetic materials are characterized by the unconventional and fascinating ability to develop transversal expansions in response to a longitudinal stretching. This physical peculiarity, which is described by negative Poisson's ratios in solid mechanics, is rarely observable in nature, but can be smoothly obtained by artificial synthesis [1–3]. The recent and increasing interest in auxetic materials is being strongly catalyzed by the compelling demand for advanced applications in aerospace, chemical, naval, nuclear, biomedical, sport engineering fields. Indeed, auxetic sheets and solids are potentially featured by a variety of functional super-capacities, including higher fracture toughness and indentation resistance, as well as augmented properties of acoustic damping and energy absorption, with respect to their conventional counterparts [4–6].

Artificial realizations of auxetic materials include polymeric or metallic foams and laminates, on the one hand, and micro-structured composites, which typically possess periodic cellular geometries (namely reticular networks, chiral lattices, re-entrant honeycombs and origami folds), on the other hand [8–10]. Leveraging their intrinsic periodicity, obeying to the well-established Floquet-Bloch theory, a promising theoretical and technological research challenge concerns the employment of chiral auxetic media as versatile elastic guides for planar optical and acoustic waves. Indeed, a proper tuning of their mechanical properties may allow the effective design of such materials as tailor-made signal propagators or – especially – selective passive filters for noise reduction and vibration mitigation [11–14]. In this respect, the high performance and versatility ensured by tunable arrays of light and flexible resonant subsystems is a promising trend coming from a multi-disciplinary cross-fertilization [15–21].

Among different chiral topologies, the anti-tetrachiral material is gaining major attention, due to its strong auxeticity, accompanied by a marked anisotropy [9, 14, 22–24]. Employing a linear beam-lattice model of the cell microstructure, the wave propagation properties of this material have been studied by means of both numerical and asymptotic tools [30]. Parametric analyses of the dispersion curves typically reveal a highly-dense spectrum, with persistent absence of band-gaps in the low-frequency range. Such shortcomings, confirmed also by continuum models and in presence of soft matrices [14] may actually limit the practical efficiency of the anti-tetrachiral materials as adjustable passive controllers against the free propagation of vibration waves with target frequencies, wavenumbers, or polarization modes.

The paper explores the possibility to develop a meta-material by introducing rigid massive inserts, locally housed by all the rings and working as undamped linear oscillators with assigned inertia and/or stiffness properties. The elastic coupling between the cell microstructure and the oscillators, if properly tuned (inertial resonators), has the potential to significantly modify the Floquet-Bloch spectrum of the material [25–28]. A suited design of this purely-mechanical behavior opens the valuable perspective to passively control the wave propagation by, first, artificially regulating the tailored opening or closure of one or more frequency band-gaps, and, second, maximizing their respective amplitudes according to optimal criteria [29].

According to this leading idea, the beam-lattice model of the anti-tetrachiral material is enriched by coupling the global dynamics of the periodic cell with the local dynamics of the resonators (Section 2). Then the coupled eigenproblem governing the wave propagation in the meta-material is formulated (Section 2.2). The effects of the resonator key-parameters (mass ratio and frequency tuning) on the dispersion curves and frequency band gaps are discussed (Section 3). These parametric studies pave the way for the analytical, although approximate, description of the enriched Floquet-Bloch spectrum by means of asymptotic perturbation techniques, suited to carry out explicit design criteria. Concluding remarks are finally drawn.

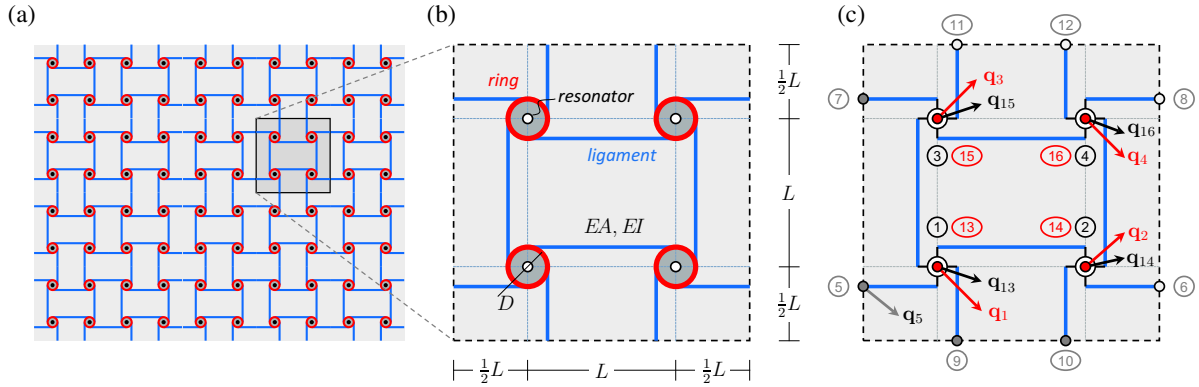

Figure 1: Anti-tetrachiral cellular meta-material: (a) pattern, (b) periodic cell, (c) beam lattice model.

2 BEAM LATTICE MODEL

Focusing on the microscopic scale, a cellular meta-material characterized by a square periodic cell, fully tiling a two-dimensional infinite domain, is considered (Figure 1a). A beam lattice model is formulated to describe the linear elasto-dynamic response of the unit cell, featured by a double geometric symmetry which realizes an anti-tetrachiral topology (Figure 1b). The internal structure, or *microstructure*, of the elementary cell is composed by four circular rings connected by twelve tangent ligaments. The *rolling-up* mechanism, responsible for the auxetic behavior, consists in the opposite-sign, iso-amplitude rotations developed by any pair of adjacent disks in-a-row (or column), when the cell is stretched along one of the symmetry axes.

A rigid body model is assumed for the massive and highly-stiff rings, possessing identical mean diameter D. The ring centers are located at the four corners of an ideal internal square, concentric with the external cell boundary. The ring small width S is considered a free parameter, allowing the independent assignment of the rigid body mass M and moment of inertia J. A linear, extensible, unshearable model of massless beam is employed for all the identical light and flexible ligaments, in the small-deformation range. As long as the beam-ring connections nominally realize perfectly-rigid joints, the natural length L of the *inner* horizontal and vertical ligaments coincide with half the side of the square cell. By virtue of the periodicity, the cell boundary crosses the midspan – and halves the natural length – of all the *outer* ligaments. Assuming the same linear elastic material (with Young's modulus E) and cross-section shape (with area A and second area moment I) for each ligament, all the beams have identical extensional EA and flexural rigidity EI. The effects of a homogeneous soft matrix, which may likely embed the microstructure [14], are neglected as first approximation.

Moving from this structural layout, a novel meta-material can be realized by supplying each ring with a light soft annular filler, hosting a central heavy circular inclusion, serving as inertial resonator with adjustable mechanical properties. All the identical inclusions are modelled as rigid disks, co-centered with the respective housing rings, with body mass M_r and moment of inertia J_r. As long as the internal coupling provided by the filler can be assumed linearly elastic, the ring-resonator differential displacements are affected by equivalent translational and rotational stiffnesses [28]. Therefore, the local (translational and rotational) motion of each resonator is essentially characterized by two natural frequencies Ω_r and Ω_θ.

Introducing a certain circular frequency Ω_c of the cellular solid as known dimensional reference, a suited minimal set of independent nondimensional parameters, sufficient to describe the inertial, elastic and geometric properties of the square periodic cell, is

$$\delta = \frac{D}{L}, \qquad \varrho^2 = \frac{I}{AL^2}, \qquad \omega_c^2 = \frac{EA}{M\Omega_c^2 L}, \qquad \chi^2 = \frac{J}{ML^2} \tag{1}$$

where ω_c stands for a frequency characterizing the beam lattice. The geometric parameter δ roughly expresses the material compositeness, measured as the linear density of the circular rings. The nondimensional form ϱ of the gyration radius of inertia accounts for the (inverse) slenderness of the ligaments. Finally, χ^2 is the rotational-to-translational mass ratio of the disks.

Together with the microstructural parameters, the meta-material is further characterized by additional nondimensional parameters, describing the properties of the local resonators

$$\gamma = \frac{\Omega_r}{\omega_c\,\Omega_c}, \qquad \alpha = \frac{M_r}{M}, \qquad \gamma_\theta = \frac{\Omega_\theta}{\omega_c\,\Omega_c}, \qquad \chi_r^2 = \frac{J_r}{M_r L^2}$$

where γ and γ_θ can be recognized as *tuning* parameters for the two resonator frequencies, α accounts for the resonator-to-ring mass ratio and χ_r^2 is the rotational-to-translational mass ratio of the resonator.

2.1 Equations of motion

According to the mechanical assumptions, the linear dynamics of the unit cell is governed by a multi-degrees-of-freedom discrete model, referred to a full set of 16 configurational nodes, located by the position vectors $\mathbf{x}_i$ (with $i = 1, ..., 16$) in the natural configuration. The actual configuration of the i-th node is described by three time-dependent components of motion, corresponding to the horizontal displacement $U_i(t)$, the vertical displacement $V_i(t)$ and the in-plane rotation $\phi_i(t)$. The nondimensional variables can be introduced

$$u_i = \frac{U_i}{L_r}, \qquad v_i = \frac{V_i}{L_r}, \qquad \tau = \Omega_r t \tag{2}$$

where L_r stands for a reference length L_r which preserves the smallness of the displacements. All the nondimensional configuration variables can be collected in the 48-by-one displacement column-vector $\mathbf{q} = (\mathbf{q}_1, ..., \mathbf{q}_i, ..., \mathbf{q}_{16})$, where the i-th nodal subvector $\mathbf{q}_i = (u_i, v_i, \phi_i)$.

Depending on the position of the lumped masses in the discrete model and with reference to the labels in Figure 1c, the model nodes can conveniently be distinguished into three subsets

i. four *internal* nodes located at the ring centroids (red nodes ①...④), whose 12 *active* displacements can be collected in the subvector $\mathbf{q}_a = (\mathbf{q}_1, \mathbf{q}_4)$

ii. eight *external* nodes located at the outer ligament midspans (gray nodes ⑤...⑫), whose 24 *passive* displacements can be cast in the subvector $\mathbf{q}_p = (\mathbf{q}_5, \mathbf{q}_{12})$

iii. four *inner* nodes located at the disk centroids (black nodes ⑬...⑯), whose 12 *resonant* displacements can be collected in the subvector $\mathbf{q}_r = (\mathbf{q}_{13}, \mathbf{q}_{16})$

The distinction remarks that the internal and inner nodes develop both nondimensional elastic $(\boldsymbol{\sigma}_a, \boldsymbol{\sigma}_r)$ *and* inertial forces $(\mathbf{f}_a, \mathbf{f}_r)$, which actively participate in the dynamic cell equilibrium. On the contrary, the external nodes can develop only elastic forces $\boldsymbol{\sigma}_p$, which partially depend on the stiffness coupling with the internal nodes, and quasi-statically balance the reactive forces $\mathbf{f}_p$ transferred by the adjacent cells. Due to the geometric assumptions, the positions of the *internal* and *inner* node sets (nodes ①...④ and ⑬...⑯) coincide in the undeformed configuration.

According to displacement/force decomposition, the nondimensional equilibrium equation governing the undamped free oscillations of the discrete model has the matrix form

$$\begin{pmatrix} \mathbf{f}_r \\ \mathbf{f}_a \\ \mathbf{0} \end{pmatrix} + \begin{pmatrix} \boldsymbol{\sigma}_r \\ \boldsymbol{\sigma}_a \\ \boldsymbol{\sigma}_p \end{pmatrix} = \begin{pmatrix} \mathbf{0} \\ \mathbf{0} \\ \mathbf{f}_p \end{pmatrix} \tag{3}$$

or, making explicit the force dependence on the nodal acceleration or displacements

$$\begin{bmatrix} \mathbf{M}_r & \mathbf{O} & \mathbf{O} \\ \mathbf{O} & \mathbf{M}_a & \mathbf{O} \\ \mathbf{O} & \mathbf{O} & \mathbf{O} \end{bmatrix} \begin{pmatrix} \ddot{\mathbf{q}}_r \\ \ddot{\mathbf{q}}_a \\ \ddot{\mathbf{q}}_p \end{pmatrix} + \begin{bmatrix} \mathbf{K}_r & -\mathbf{K}_r & \mathbf{O} \\ -\mathbf{K}_r & \mathbf{K}_{aa}+\mathbf{K}_r & \mathbf{K}_{ap} \\ \mathbf{O} & \mathbf{K}_{pa} & \mathbf{K}_{pp} \end{bmatrix} \begin{pmatrix} \mathbf{q}_r \\ \mathbf{q}_a \\ \mathbf{q}_p \end{pmatrix} = \begin{pmatrix} \mathbf{0} \\ \mathbf{0} \\ \mathbf{f}_p \end{pmatrix} \tag{4}$$

where dot indicates differentiation with respect to the τ-time and $\mathbf{O}$ stands for empty matrices.

Focusing on the micro-structural matrices, the *global* mass submatrix $\mathbf{M}_a$ is diagonal, as far as a lumped mass description is assumed. The symmetric submatrices $\mathbf{K}_{aa}$ and $\mathbf{K}_{pp}$ account for the *global* stiffness of the internal and external nodes, respectively. The rectangular submatrix $\mathbf{K}_{ap} = \mathbf{K}_{pa}^{\top}$ expresses the elastic *global* coupling among the internal and external nodes. A parametric expression of these matrices can be found in [30]. Focusing on the resonators, both the *local* mass and stiffness submatrices $\mathbf{M}_r$ and $\mathbf{K}_r$ are diagonal. The submatrix $\mathbf{K}_r$ accounts also for the *global-local* coupling between the inner and internal nodes.

2.2 Free wave propagation

The free wave propagation along the bi-dimensional cell domain can be studied according to the Floquet-Bloch theory [31–33]. Moving in the $\mathbf{k}$-transformed space the active ($j = 1...4, 13...16$) and passive displacements and passive force vectors assume the representations

$$\mathbf{q}_j = \tilde{\mathbf{q}}_j \, \mathrm{e}^{\mathrm{i}\,\mathbf{k}\cdot\mathbf{x}_j}, \qquad \mathbf{q}_p = \mathbf{F}_p \tilde{\mathbf{q}}_p, \qquad \mathbf{f}_p = \mathbf{F}_p \tilde{\mathbf{f}}_p \tag{5}$$

where i denotes the imaginary unit, $\mathbf{k} = (k_1, k_2)$ is the (dimensional) wavevector and the block diagonal matrix $\mathbf{F}_p = \mathrm{diag}[\,\mathbf{I}\,\mathrm{e}^{\mathrm{i}\,\mathbf{k}\cdot\mathbf{x}_5}, ..., \mathbf{I}\,\mathrm{e}^{\mathrm{i}\,\mathbf{k}\cdot\mathbf{x}_{12}}\,]$ with $\mathbf{I}$ being the three-by-three unit matrix.

The passive displacement and force vector can be ordered and partitioned as $\mathbf{q}_p = (\mathbf{q}_p^-, \mathbf{q}_p^+)$, $\mathbf{f}_p = (\mathbf{f}_p^-, \mathbf{f}_p^+)$ to separate the variable pairs $(\mathbf{q}_p^-, \mathbf{f}_p^-)$ belonging to the left/bottom cell boundary (composed by the external nodes ⑤,⑦,⑨,⑩) from the variable pairs $(\mathbf{q}_p^+, \mathbf{f}_p^+)$ belonging to the right/top boundary (composed by the external nodes ⑥,⑧,⑪,⑫). Extending the same partition to the respective transformed variables, the equation (5) can be written

$$\mathbf{q}_p^- = \mathbf{F}_p^- \tilde{\mathbf{q}}_p^-, \qquad \mathbf{q}_p^+ = \mathbf{F}_p^+ \tilde{\mathbf{q}}_p^+, \qquad \mathbf{f}_p^- = \mathbf{F}_p^- \tilde{\mathbf{f}}_p^-, \qquad \mathbf{f}_p^+ = \mathbf{F}_p^+ \tilde{\mathbf{f}}_p^+, \tag{6}$$

where, based on the decomposition, the matrices $\mathbf{F}_p^- = \mathrm{diag}[\,\mathbf{I}\,\mathrm{e}^{\mathrm{i}\,\mathbf{k}\cdot\mathbf{x}_5}, \mathbf{I}\,\mathrm{e}^{\mathrm{i}\,\mathbf{k}\cdot\mathbf{x}_7}, \mathbf{I}\,\mathrm{e}^{\mathrm{i}\,\mathbf{k}\cdot\mathbf{x}_9}, \mathbf{I}\,\mathrm{e}^{\mathrm{i}\,\mathbf{k}\cdot\mathbf{x}_{10}}]$ and $\mathbf{F}_p^+ = \mathrm{diag}[\,\mathbf{I}\,\mathrm{e}^{\mathrm{i}\,\mathbf{k}\cdot\mathbf{x}_6}, \mathbf{I}\,\mathrm{e}^{\mathrm{i}\,\mathbf{k}\cdot\mathbf{x}_8}, \mathbf{I}\,\mathrm{e}^{\mathrm{i}\,\mathbf{k}\cdot\mathbf{x}_{11}}, \mathbf{I}\,\mathrm{e}^{\mathrm{i}\,\mathbf{k}\cdot\mathbf{x}_{12}}\,]$.

Imposing the periodicity conditions on the transformed variables ($\tilde{\mathbf{q}}_p^+ = \tilde{\mathbf{q}}_p^-$ and $\tilde{\mathbf{f}}_p^+ = -\tilde{\mathbf{f}}_p^-$), the free wave propagation throughout the cell domain between the two complementary boundaries is governed by the quasi-periodicity conditions on the anti-transformed variables

$$\mathbf{q}_p^+ = \mathbf{L}\mathbf{q}_p^-, \qquad \mathbf{f}_p^+ = -\mathbf{L}\mathbf{f}_p^- \tag{7}$$

where, following from the equations (6), the block diagonal transfer matrix reads

$$\mathbf{L} = \mathrm{diag}\left[\mathrm{e}^{\mathrm{i}\,\mathbf{k}\cdot\mathbf{d}_{56}}\,\mathbf{I}, \mathrm{e}^{\mathrm{i}\,\mathbf{k}\cdot\mathbf{d}_{78}}\,\mathbf{I}, \mathrm{e}^{\mathrm{i}\,\mathbf{k}\cdot\mathbf{d}_{911}}\,\mathbf{I}, \mathrm{e}^{\mathrm{i}\,\mathbf{k}\cdot\mathbf{d}_{1012}}\,\mathbf{I}\right] \tag{8}$$

and $\mathbf{d}_{ij} = \mathbf{x}_j - \mathbf{x}_i$ represents the vector connecting the i-th and the j-th external nodes.

Consistently with the passive displacement and force decomposition, and imposing the quasi-periodicity conditions (8), the lower (quasi-static) part of equation (4) reads

$$\begin{bmatrix} \mathbf{K}_{pa}^{-} \\ \mathbf{K}_{pa}^{+} \end{bmatrix} \mathbf{q}_a + \begin{bmatrix} \mathbf{K}_{pp}^{=} & \mathbf{K}_{pp}^{\mp} \\ \mathbf{K}_{pp}^{\pm} & \mathbf{K}_{pp}^{\#} \end{bmatrix} \begin{bmatrix} \mathbf{I} \\ \mathbf{L} \end{bmatrix} \mathbf{q}_p^{-} = \begin{bmatrix} \mathbf{I} \\ -\mathbf{L} \end{bmatrix} \mathbf{f}_p^{-} \tag{9}$$

with $\mathbf{I}$ being now the twelve-by-twelve unit matrix. This equation can be solved to express the passive variables as slave functions of the master active displacements, yielding

$$\mathbf{q}_p^{-} = \mathbf{R}\big(\mathbf{K}_{pa}^{+} + \mathbf{L}\mathbf{K}_{pa}^{-}\big)\mathbf{q}_a, \qquad \mathbf{f}_p^{-} = \big(\mathbf{K}_{pa}^{-} + \big(\mathbf{K}_{pp}^{=} + \mathbf{K}_{pp}^{\mp}\mathbf{L}\big)\mathbf{R}\big(\mathbf{K}_{pa}^{+} + \mathbf{L}\mathbf{K}_{pa}^{-}\big)\big)\mathbf{q}_a \tag{10}$$

where the k-dependent matrix $\mathbf{R} = -\big(\mathbf{L}\mathbf{K}_{pp}^{\mp}\mathbf{L} + \mathbf{L}\mathbf{K}_{pp}^{=} + \mathbf{K}_{pp}^{\#}\mathbf{L} + \mathbf{K}_{pp}^{\pm}\big)^{-1}$ is diagonal.

Similarly, the imposition of the quasi-periodicity conditions to the upper (dynamic) part of the equation (4) leads to a coupled equation which, after *condensation* of the passive variables by virtue of the enslaving relations (11), depends on the active variables only

$$\begin{bmatrix} \mathbf{M}_r & \mathbf{O} \\ \mathbf{O} & \mathbf{M}_a \end{bmatrix} \begin{pmatrix} \ddot{\mathbf{q}}_r \\ \ddot{\mathbf{q}}_a \end{pmatrix} + \begin{bmatrix} \mathbf{K}_r & -\mathbf{K}_r \\ -\mathbf{K}_r & \mathbf{K}_r + \mathbf{K}_a \end{bmatrix} \begin{pmatrix} \mathbf{q}_r \\ \mathbf{q}_a \end{pmatrix} = \begin{pmatrix} \mathbf{0} \\ \mathbf{0} \end{pmatrix} \tag{11}$$

where the condensed stiffness matrix $\mathbf{K}_a = \mathbf{K}_{aa} + (\mathbf{K}_{ap}^{-} + \mathbf{K}_{ap}^{+}\mathbf{L})\mathbf{R}(\mathbf{K}_{pa}^{+} + \mathbf{L}\mathbf{K}_{pa}^{-})$, with the symmetries $\mathbf{K}_{ap}^{-} = (\mathbf{K}_{pa}^{-})^{\top}$ and $\mathbf{K}_{ap}^{+} = (\mathbf{K}_{pa}^{+})^{\top}$ is known to be Hermitian and is derived in [30].

As brief discussion, the upper part of equation (11) can still be recognized to govern the local resonator dynamics, whereas the lower part governs the global dynamics of the cell microstructure. It is worth noting that the passive variable condensation, including the enforcement of the quasi-periodicity, is not mathematically affected by the resonator presence. Indeed, the condensed *global* stiffness matrix $\mathbf{K}_g = (\mathbf{K}_r + \mathbf{K}_a)$ of the meta-material is not formally different from the matrix $\mathbf{K}_a$ governing the wave propagation in the resonator-free material, apart for the mere addiction of the *local* stiffness term $\mathbf{K}_r$. Conversely, the uncoupled global dynamics the resonator-free material can be restored by simply zeroing the local matrices $\mathbf{M}_r$ and $\mathbf{K}_r$. Physically, this remark can immediately be justified by the absence of any internal coupling between the resonant active variables $\mathbf{q}_r$ and the condensed passive variables $\mathbf{q}_p$.

Denoting ω the unknown nondimensional frequency, the harmonic monofrequent solution $\mathbf{q}_a = \mathbf{F}_a\boldsymbol{\psi}_a\,\mathrm{e}^{\mathrm{i}\,\omega\tau}$ and $\mathbf{q}_r = \mathbf{F}_r\boldsymbol{\psi}_r\,\mathrm{e}^{\mathrm{i}\,\omega\tau}$ can be imposed in the equation (11). Eliminating the dependence on time, an eigenproblem in the unknown eigenvalues $\lambda = \omega^2/\omega_c^2$ and eigenvectors $\boldsymbol{\psi} = (\boldsymbol{\psi}_r, \boldsymbol{\psi}_a)$ can be stated in the non-standard form $(\mathbf{K} - \lambda\mathbf{M})\,\mathbf{F}\boldsymbol{\psi} = \mathbf{0}$, or more explicitly

$$\left(\begin{bmatrix} \mathbf{K}_r & -\mathbf{K}_r \\ -\mathbf{K}_r & \mathbf{K}_a \end{bmatrix} - \lambda \begin{bmatrix} \mathbf{M}_r & \mathbf{O} \\ \mathbf{O} & \mathbf{M}_a \end{bmatrix}\right) \begin{bmatrix} \mathbf{F}_r \\ \mathbf{F}_a \end{bmatrix} \boldsymbol{\psi} = \begin{pmatrix} \mathbf{0} \\ \mathbf{0} \end{pmatrix} \tag{12}$$

where the diagonal block matrices $\mathbf{F}_r = \mathbf{F}_a = \mathrm{diag}[\,\mathbf{I}\,\mathrm{e}^{\mathrm{i}\,\mathbf{k}\cdot\mathbf{x}_1}, ..., \mathbf{I}\,\mathrm{e}^{\mathrm{i}\,\mathbf{k}\cdot\mathbf{x}_4}\,]$.

The eigenproblem solution gives twenty-four real-valued eigenvalues λ_i (or frequencies ω_i), sorted in ascending order. It is worth remarking that, owing to the Hermitian property, the $\mathbf{K}$-matrix is certainly non-defective, that is, possesses a complete eigenspace spanned by twenty-four proper eigenvectors. Therefore, each eigenvalue λ_i has coincident algebraic and geometric multiplicity m_i and corresponds to a complex-valued eigenvector $\boldsymbol{\psi}_i$, collecting the non-passive eigencomponents $\boldsymbol{\psi}_{ri}$ and $\boldsymbol{\psi}_{ai}$ only. The passive eigencomponents depend on the active eigencomponents through the quasi-static relations $\boldsymbol{\psi}_{pi}^{-} = \mathbf{R}\big(\mathbf{K}_{pa}^{+} + \mathbf{L}\mathbf{K}_{pa}^{-}\big)\boldsymbol{\psi}_{ai}$ and $\boldsymbol{\psi}_{pi}^{+} = \mathbf{L}\boldsymbol{\psi}_{pi}^{-}$.

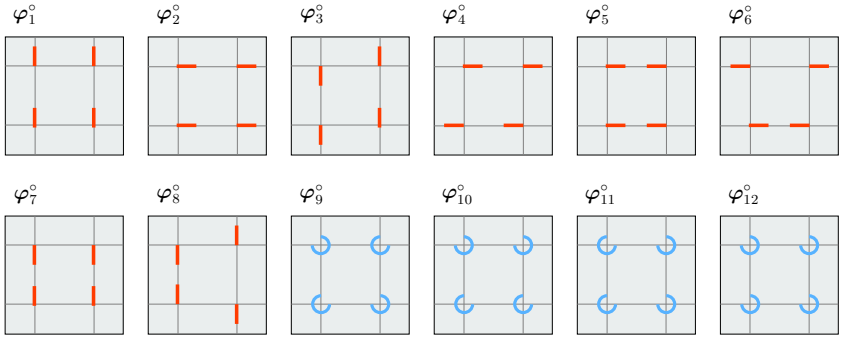

Figure 2: Stationary translational (red) or rotational (blue) modes $\boldsymbol{\psi}_{ai}$ of the anti-tetrachiral material (a omitted).

3 FLOQUET-BLOCH SPECTRUM

Fixed certain parameter values for the beam-lattice model and the resonators, the twenty-four eigenvalues (or frequencies) and the corresponding eigenvectors can be determined under variation of the nondimensional wavevector $\mathbf{b} = (\beta_1, \beta_2)$, composed of the wavenumbers

$$\beta_1 = \mathbf{k} \cdot \mathbf{d}_{56} = \mathbf{k} \cdot \mathbf{d}_{78}, \qquad \beta_2 = \mathbf{k} \cdot \mathbf{d}_{911} = \mathbf{k} \cdot \mathbf{d}_{1012} \tag{13}$$

in the square Brillouin domain $\mathcal{D} = [-\pi, \pi] \times [-\pi, \pi]$. According to the Floquet-Bloch theory [31–33], this investigation can be focused on the two edges

$$\mathcal{B}_1 = \{\beta_1 \in [0, \pi], \beta_2 = 0\}, \qquad \mathcal{B}_{12} = \{\beta_1 = \beta_2 \in [0, \pi]\} \tag{14}$$

which bound the irreducible triangular zone of the $\mathcal{D}$-domain and are spanned by the abscissae β_1 and $\beta_{12} = (\beta_1^2 + \beta_2^2)^{1/2}$, respectively. The corresponding ω-frequent vibration waves propagate through the periodic material along the horizontal direction (with β_1-wavenumber ranging in $[0, \pi]$) and diagonal direction (with β_{12}-wavenumber ranging in $[0, \sqrt{2}\pi]$).

The frequency loci versus the variable wavenumber constitute the Floquet-Bloch spectrum, composed of twenty-four dispersion curves for the meta-material or twelve dispersion curves for the resonator-free material (as can be carried out by setting $\mathbf{M}_r = \mathbf{K}_r = \mathbf{O}$). The curve *roots*, located at the $\mathcal{D}$-origin ($\beta_1 = \beta_2 = 0$), correspond to the quasi-periodicity conditions (7) degenerating into conditions of standard periodicity. Therefore, the corresponding eigenpairs $(\lambda^\circ, \boldsymbol{\varphi}^\circ)$ can be interpreted as the natural frequencies, possibly null, and (real-valued) vibration modes of the single elementary cell in the free stationary harmonic oscillation of the periodic system. In the absence of resonators, these modes are participated only by an homogeneous subset of active displacements (Figure 2). so that they can be classified as *translational modes*, if contributed by the four horizontal or the four vertical components, or *rotational modes*, if contributed by the four rotation components. With minor abuse of nomenclature, the same classification can be extended to the $\mathbf{b}$-dependent eigenvectors, which can be interpreted as polarization modes of the propagating wave, characterized by a certain (not null) wavenumber.

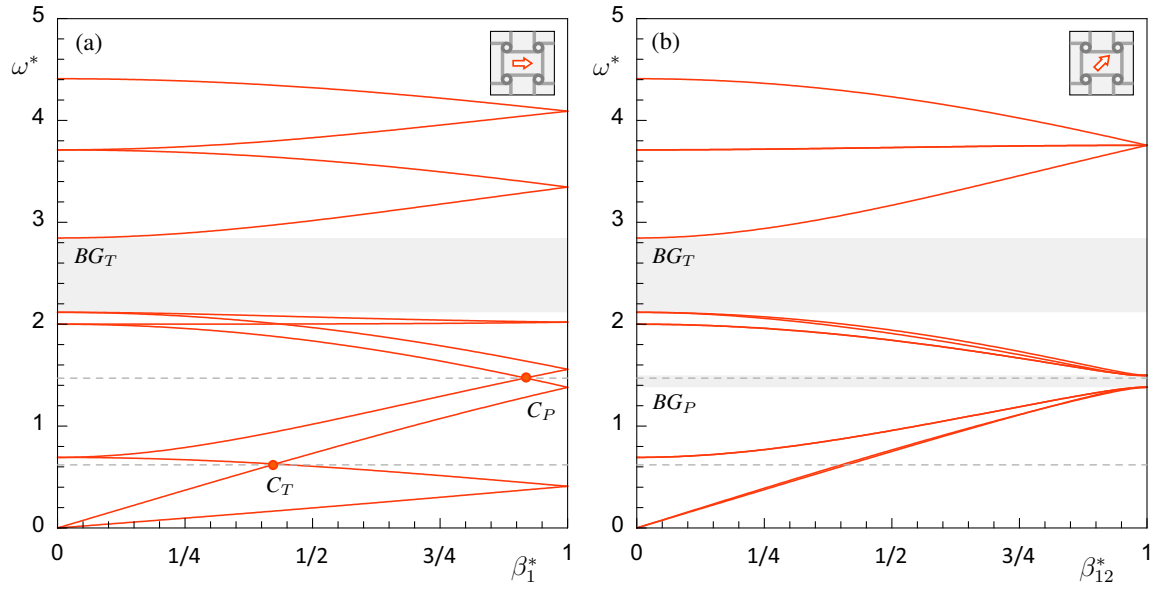

Figure 3: Floquet-Bloch spectrum ($\omega* = \omega/\omega_c$) of the anti-tetrachiral material (without resonators): (a) horizontal and (b) diagonal direction of wave propagation ($\beta_1^* = \beta_1/\pi$, $\beta_{12}^* = \beta_{12}/(\sqrt{2}\pi)$).

3.1 Parametric analysis

In the absence of resonators, the Floquet-Bloch spectrum is presented in Figure 3 for a set of parameter values ($\chi^2 = 1/81, \delta = 1/10, \varrho^2 = 1/100$). For both the propagation directions, the low-frequency (namely ω_1-ω_8) and high-frequency (namely ω_9-ω_{12}) ranges are separated from each other by the total band gap BG_T, and the respective polarizations are systematically dominated by translational and rotational modes, respectively. Some parametric analyses show that, as long as the two frequency ranges remains well-separated, the translational frequency curves (rigorously, the curves related to the frequencies of translational modes) undergo only minor qualitative and quantitative changes for slight variations of the parameter set $(\varrho^2, \chi^2, \delta)$. On the contrary, the rotational frequencies (rigorously, the curves related to the frequencies of rotational modes) strongly depend on the δ and χ parameters, with an approximately linear law of direct and inverse proportionality, respectively. Physically, this remark states that the amplitude of the total band gap BG_T can be amplified/reduced by modifying the ring density (higher/lower δ-values) or their rotational-to-translational mass ratio (lower/higher χ^2-values). For instance, the band gap can be verified to close (null amplitude) for $\chi^2 \geq 1/36$.

As major remark, the material does not present low-frequency total band gaps, neither they can be obtained for a different, generic parameter set. This persistent scenario is a direct consequence of the high spectral density characterizing the translational frequencies, together with the large number of crossing points between their dispersion curves. Looking at waves propagating along the diagonal direction (Figure 3b), the small-amplitude partial band-gap BG_P can be found at low-frequencies, ranging between two translational-translation curves. It can be verified that this gap occurs in the direction of minimum auxeticity of the material, consistently with the findings of [14]. Fixed the other parameter, the gap amplitude A_{12} can be moderately increased by an increment of the δ-parameter, up to $A_{12} \simeq 0.250$.

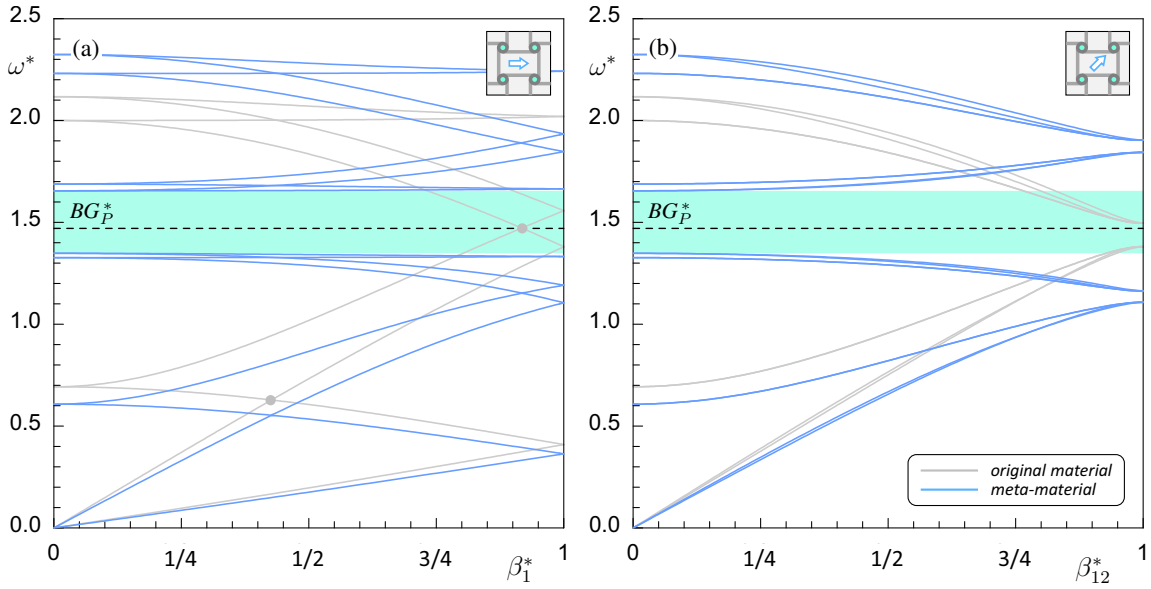

Figure 4: Low-frequency Floquet-Bloch spectrum ($\omega* = \omega/\omega_c$) of the meta-material ($\gamma = 148/100$): (a) horizontal and (b) diagonal direction of wave propagation ($\beta_1^* = \beta_1/\pi$, $\beta_{12}^* = \beta_{12}/(\sqrt{2}\pi)$).

3.2 Effects of the local resonators

The strong potential recognized to micro-oscillator arrays in preventing the wave propagation through periodic lattices can be explained by the effective negative values of mass density achievable in the equivalent elastic continua [25, 26]. Inter-oscillator distances lower than the typical wavelengths let the meta-material internally resonate in the low-frequency range, where band gaps may open in the Floquet-Bloch spectrum, in correspondence with the tunable natural frequencies of the oscillators (resonators). The present study is focused on two different tasks

i. check whether a proper tuning of the meta-material resonators (through the γ-parameter) allow the opening of total band gaps, by either the widening of an existing partial band gap or the transformation of a crossing point into a veering between adjacent curves,

ii. verify the possibility to finely control (through the α-parameter) the total band-gap amplification/deamplification, in order to quantitatively evaluate the meta-material potential in terms of achievable performance range against undesired wave propagation.

To the former task, the oscillator-to-ring mass can be tentatively assigned to the reference value $\alpha = 1/2$, which optimizes the resonator performance in similar chiral meta-materials [29]. First, the partial-to-total widening of the low-frequency band gap BG_P is challenged. The crossing C_P between the forth and fifth dispersion curves, which closes the band gap in the horizontal propagation direction, is pointed as target frequency by tuning $\gamma = 148/100$ (corresponding to the upper dashed line in Figure 3). The efficiency of the resonator action is confirmed by the low-frequency Floquet-Bloch spectrum of the meta-material (Figure 4). Indeed, a new total band BG_P^*, with almost $\mathbf{b}$-independent amplitude $A_1 = A_{12} \simeq 0.300$, rises up and lies just across the tuned frequency. The original crossing point is removed by a strong softening/hardening effect, consisting in the downward/upward frequency shifting of the previously intersecting curves (gray lines). The band gap opening is not compromised by the local densification of the spectrum owing to the doubled dimension of the meta-material model.

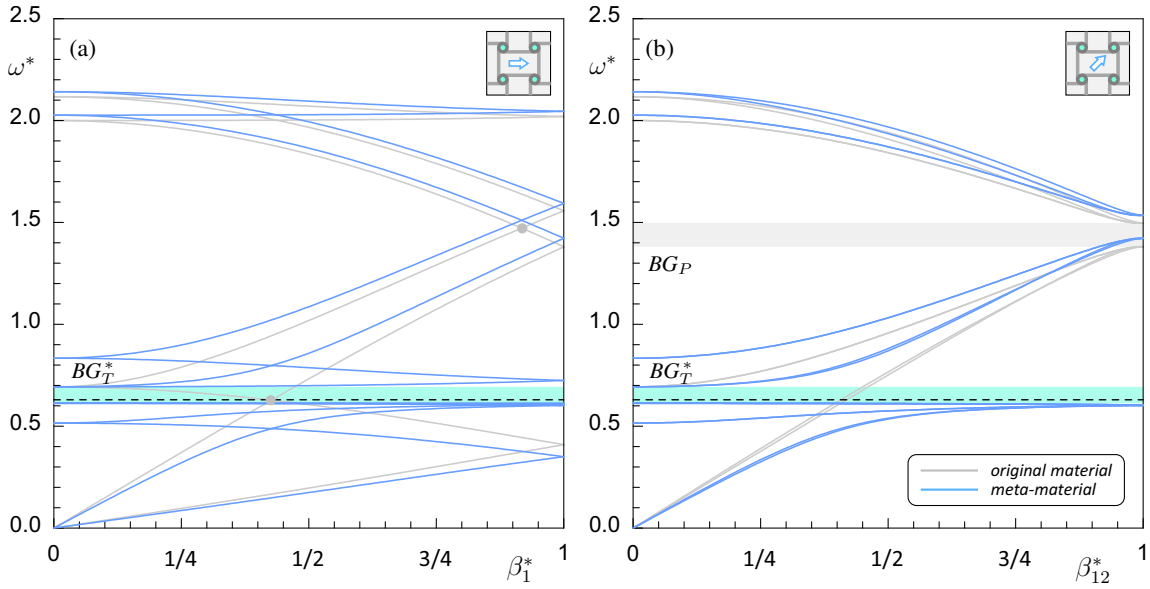

Figure 5: Low-frequency Floquet-Bloch spectrum of the anti-tetrachiral meta-material ($\gamma = 62/100$): (a) horizontal and (b) diagonal direction of wave propagation ($\beta_1^* = \beta_1/\pi$, $\beta_{12}^* = \beta_{12}/(\sqrt{2}\pi)$).

Second, the crossing C_T between the second and third dispersion curves, which characterizes the horizontal propagation direction, is pointed as target frequency by tuning $\gamma = 62/100$ (corresponding to the lower dashed line in Figure 3). Again, the resonator action successes in opening a low-frequency total band BG_P^*, with almost $\mathbf{b}$-independent amplitude $A_1 = A_{12} \simeq 0.037$, lying across the tuned frequency (Figure 5). The band gap is provided by a strong linear interaction among the new spectrum curves and the previously intersecting curves (gray lines), which are forced to veer away form their original crossing point.

To the latter task, a few parametric analyses have been carried out under variation of the resonator-to-ring mass, without changes in the tuning parameters (Table 1). The results tend to confirm that the total band gap amplitudes are $\mathbf{b}$-independent ($A_1 = A_{12}$) and that – fixed the resonator mass – larger band gap are achievable at higher tuning frequencies. Finally, the band gap amplitudes are found to grow up with the increments of the resonator mass. In this respect, the trend of the mass-to-amplitude ratios suggests an underlying quadratic relationship which could be investigated by means of local analyses based on perturbation methods.

Table 1: Amplitudes of the low-frequency band-gaps obtainable in the anti-tetrachiral meta-material.

	PERIODIC MATERIAL ($\omega^* \simeq 148/100$)			PERIODIC MATERIAL ($\omega^* \simeq 62/100$)		
	A_1	A_{12}	Description	A_1	A_{12}	Description
	–	0.114	Partial	–	–	Absent
	META-MATERIAL ($\gamma = 148/100$)			META-MATERIAL ($\gamma = 62/100$)		
α	A_1	A_{12}	Description	A_1	A_{12}	Description
1/4	0.086	0.086	Total	0.021	0.021	Total
1/3	0.148	0.148	Total	0.037	0.037	Total
1/2	0.307	0.307	Total	0.080	0.080	Total
2/3	0.501	0.501	Total	0.138	0.138	Total

4 CONCLUSIONS

A parametric beam-lattice model has been formulated to describe the linear planar dynamics of the unit cell which characterizes the periodic microstructure of the auxetic anti-tetrachiral material. The persistent absence of low-frequency band gaps in the Floquet-Bloch spectrum has been verified. This lack limits the smart functionalities of passive noise suppression and vibration filtering of the material, when it is used as elastic waveguide. The transformation into a meta-material, by introducing local undamped resonators with flexible properties of tunable *frequency* and selectable *mass* ratio, has demonstrated its potential in strongly modifying the original low-frequency band structure. In particular, a tailor-made design of the resonator parameters has allowed the widening of an existing partial band gap, as well as the opening of a new band gap across the tuned frequency, with adjustable amplitude depending on the selected mass.

References

[1] R. Lakes, Deformation mechanisms in negative Poisson's ratio materials: structural aspects. *Journal of Materials Science* **26**(9) 2287–2292, 1991.

[2] A. Alderson, K. Alderson, Auxetic materials. *Proceedings of the Institution of Mechanical Engineers, Part G: Journal of Aerospace Engineering* **221**(4) 565–575, 2007.

[3] Y. Prawoto, Seeing auxetic materials from the mechanics point of view: a structural review on the negative Poisson's ratio. *Computational Materials Science* **58** 140–153, 2012.

[4] D. Prall, R. Lakes, Properties of a chiral honeycomb with a Poisson's ratio of-1. *International Journal of Mechanical Sciences* **39**(3) 305–314, 1997.

[5] J. Dirrenberger, S. Forest, D. Jeulin, Effective elastic properties of auxetic microstructures: anisotropy and structural applications. *International Journal of Mechanics and Materials in Design* **9**(1) 21–33,2013.

[6] A. Bacigalupo, L. Gambarotta, Homogenization of periodic hexa-and tetrachiral cellular solids. *Composite Structures* **116** 461–476, 2014.

[7] J.E. Cadman, S. Zhou, Y. Chen, Q. Li, On design of multi-functional microstructural materials. *Journal of Materials Science* **48**(1) 51–66, 2013.

[8] O. Sigmund, S. Torquato, I. Aksay, On the design of 1-3 piezocomposites using topology optimization. *Journal of Materials Research* **13**(4) 1038–1048, 1998.

[9] A. Alderson, K. Alderson, D. Attard, K. Evans, R. Gatt, J. Grima, W. Miller, N. Ravirala, C. Smith, K. Zied, Elastic constants of 3-, 4- and 6-connected chiral and anti-chiral honeycombs subject to uniaxial in-plane loading. *Composites Science and Technology* **70**(7) 1042–1048, 2010.

[10] L. Yang, O. Harrysson, H. West, D. Cormier, Mechanical properties of 3d re-entrant honeycomb auxetic structures realized via additive manufacturing. *International Journal of Solids and Structures* **69-70** 475–490, 2015.

[11] M. Ruzzene, F. Scarpa, Directional and band-gap behavior of periodic auxetic lattices. *Physica Status Solidi (b)* **242**(3) 665–680, 2005.

[12] A. Spadoni, M. Ruzzene, S. Gonella, F. Scarpa, Phononic properties of hexagonal chiral lattices. *Wave Motion* **46**(7) 435–450, 2009.

[13] K. Tee, A. Spadoni, F. Scarpa, M. Ruzzene, Wave propagation in auxetic tetrachiral honeycombs. *Journal of Vibration and Acoustics* **132**(3) 031007, 2010.

[14] A. Bacigalupo, M.L. De Bellis, Auxetic anti-tetrachiral materials: equivalent elastic properties and frequency band-gaps. *Composite Structures* **131** 530–544, 2015.

[15] V. Gattulli, F. Potenza, M. Lepidi, Damping performance of two simple oscillators coupled by a visco-elastic connection. *Journal of Sound and Vibration* **332**(26) 6934–6948, 2013.

[16] I. Venanzi, F. Ubertini, A.L Materazzi, Optimal design of an array of active tuned mass dampers for wind-exposed high-rise buildings. *Structural Control and Health Monitoring* **20**(6) 903–917, 2013.

[17] M. Lepidi, Multi-parameter perturbation methods for the eigensolution sensitivity analysis of nearly-resonant non-defective multi-degree-of-freedom systems. *Journal of Sound and Vibration* **332**(4) 1011–1032, 2013.

[18] A. Casalotti, A. Arena, W. Lacarbonara, Mitigation of post-flutter oscillations in suspension bridges by hysteretic tuned mass dampers. *Engineering Structures* **69** 62–71, 2014.

[19] I. Venanzi, Robust optimal design of tuned mass dampers for tall buildings with uncertain parameters. *Structural and Multidisciplinary Optimization* **51**(1) 239–250, 2015.

[20] M. Lepidi, G. Piccardo, Aeroelastic stability of a symmetric multi-body section model. *Meccanica* **50**(3) 731–749, 2015.

[21] F. Tubino, G. Piccardo, Tuned Mass Damper optimization for the mitigation of human-induced vibrations of pedestrian bridges. *Meccanica* **50**(3) 809–824,2015.

[22] J.N. Grima, R. Gatt, P.-S. Farrugia, On the properties of auxetic meta-tetrachiral structures. *Physica Status Solidi (b)* **245**(3) 511–520, 2008.

[23] Y. Chen, F. Scarpa, Y. Liu, J. Leng, Elasticity of anti-tetrachiral anisotropic lattices. *International Journal of Solids and Structures* **50**(6) 996–1004, 2013.

[24] R. Gatt, D. Attard, P.-S. Farrugia, K.M. Azzopardi, L. Mizzi, J.-P. Brincat, J.N. Grima, A realistic generic model for anti-tetrachiral systems. *Physica Status Solidi (b)* **250**(10) 2012–2019, 2013.

[25] H. Huang, C. Sun, G. Huang, On the negative effective mass density in acoustic metamaterials. *International Journal of Engineering Science* **47**(4) 610–617, 2009.

[26] H. Huang, C. Sun, Wave attenuation mechanism in an acoustic metamaterial with negative effective mass density. *New Journal of Physics* **11**(1) 013003, 2009.

[27] D. Bigoni, S. Guenneau, A.B. Movchan, M. Brun, Elastic metamaterials with inertial locally resonant structures: Application to lensing and localization. *Physical Review B* **87**(17), 174303, 2013.

[28] A. Bacigalupo, L. Gambarotta, Simplified modelling of chiral lattice materials with local resonators. *International Journal of Solids and Structures* **83** 126–141, 2016.

[29] A. Bacigalupo, M. Lepidi, G. Gnecco, L. Gambarotta, Optimal design of auxetic hexachiral metamaterials with local resonators. *Smart Materials and Structures*, **25**(5), 054009, 2016.

[30] A. Bacigalupo, M. Lepidi, High-frequency parametric approximation of the Floquet-Bloch spectrum for anti-tetrachiral materials. *International Journal of Solids and Structures*, under review 2016.

[31] L. Brillouin, Wave propagation in periodic structures: electric filters and crystal lattices. *Courier Corporation*, 2003.

[32] I.V. Andrianov, V.I. Bolshakov, V.V. Danishevs'kyy, D. Weichert, Higher order asymptotic homogenization and wave propagation in periodic composite materials. *Proc. Royal Society A: Mathematical, Physical and Engineering Sciences* **464**(2093) 1181–1201, 2008.

[33] A. Bacigalupo, L Gambarotta, Second-gradient homogenized model for wave propagation in heterogeneous periodic media. *International Journal of Solids and Structures* **51**(5) 1052–1065, 2014.